Dissociative electron attachment and electron-impact resonant dissociation of vibrationally excited O_2 molecules

V. Laporta,[1,2,*] R. Celiberto,[1,3] and J. Tennyson[2]

[1]*Istituto di Metodologie Inorganiche e dei Plasmi, CNR, 70125 Bari, Italy*

[2]*Department of Physics and Astronomy, University College London, London WC1E 6BT, United Kingdom*

[3]*Dipartimento di Ingegneria Civile, Ambientale, del Territorio, Edile e di Chimica, Politecnico di Bari, 70125 Bari, Italy*

(Received 22 May 2014; published 5 January 2015)

State-by-state cross sections for dissociative electron attachment and electron-impact dissociation for molecular oxygen are computed using *ab initio* resonance curves calculated with the *R*-matrix method. When O_2 is in its vibrational ground state, the main contribution for both processes comes from the $^2\Pi_u$ resonance state of O_2^- but with a significant contribution from the $^4\Sigma_u^-$ resonant state. Vibrational excitation leads to an increased contribution from the low-lying $^2\Pi_g$ resonance, greatly increased cross sections for both processes, and the threshold moving to lower energies. These results provide important input for models of O_2-containing plasmas in nonequilibrium conditions.

DOI: 10.1103/PhysRevA.91.012701 PACS number(s): 34.80.Ht, 34.80.Gs, 52.20.Fs

I. INTRODUCTION

Molecular oxygen is a major component of the Earth's atmosphere and is fundamental for life. It plays an important role in many natural and technological processes. In this paper we focus on the ability of low-energy electrons to dissociate molecular oxygen, in its fundamental electronic state, by means of resonant scattering. In particular we consider the state-by-state processes of dissociative electron attachment (DEA),

$$e^- + O_2(X\,^3\Sigma_g^-; v) \rightarrow O_2^{-*} \rightarrow O^-(^2P) + O(^3P)\,, \quad (1)$$

and electron impact dissociation (EID),

$$e^- + O_2(X\,^3\Sigma_g^-; v) \rightarrow O_2^{-*} \rightarrow e^- + 2\,O(^3P)\,, \quad (2)$$

for each oxygen vibrational level v. The threshold for process (1) is 3.64 eV, corresponding to the asymptotic energy of O and O^- fragments from level $v = 0$, whereas that for process (2) corresponds to an oxygen dissociation of 5.11 eV.

Such collisions are important for studying phenomena occurring in the upper atmosphere, re-entry physics, electrical discharges, and plasma chemistry. DEA is the principal mechanisms, in molecular plasmas, for forming negative ions from neutral molecules; the inverse process represents associative detachment. Although significant theoretical and experimental effort has been invested in characterizing electron-O_2 cross sections [1], information is only available for the vibrational ground state of O_2 for which both processes have rather small cross sections. Here, we will show that DEA and EID processes become much more important for vibrationally excited oxygen, as the corresponding cross sections increases by orders of magnitude with the excitation of the molecule. These cross sections represent fundamental input quantities in kinetics models of oxygen-containing nonequilibrium plasmas, in which high-lying vibrational levels of molecules can be hugely populated.

This paper is organized as follows: In Sec. II we give a brief account and numerical details of the adopted theoretical models for the calculation of the potential energy curves and of the description of the nuclear dynamics. The results are illustrated in Sec. III, and the concluding remarks are given in Sec. IV.

II. THEORETICAL MODEL

Many low-energy electron-molecule scattering processes are dominated by resonances. For molecular oxygen these processes can be quantitatively understood in terms of four low-lying O_2^- resonances of symmetries $^2\Pi_g$, $^2\Pi_u$, $^4\Sigma_u^-$, and $^2\Sigma_u^-$. The first calculations were made by Noble *et al.* [2], who used the *R*-matrix method [3] to determine the positions and widths of these four resonances. The O_2 target was represented using nine states, corresponding to the orbital configurations [core]$1\pi_u^4 1\pi_g^2$ and [core]$1\pi_u^3 1\pi_g^3$. The scattering T matrix was calculated in the fixed-nuclei approximation for the internuclear distance range $[1.85, 3.5]a_0$, using the configurations [core]$1\pi_u^4 1\pi_g^3$ ($^2\Pi_g$), [core]$1\pi_u^3 1\pi_g^4$ ($^2\Pi_u$), [core]$1\pi_u^4 1\pi_g^2 3\sigma_u$ ($^4\Sigma_u^-$), and [core]$1\pi_u^4 1\pi_g^2 3\sigma_u$ ($^2\Sigma_u^-$) for energies up to 15 eV.

In our previous paper on state-to-state cross sections for resonant vibrational excitation (RVE) for electron-oxygen scattering [4], we extended Noble *et al.*'s calculations toward larger internuclear distances using the quantum chemistry code MOLPRO [5]. We used a multireference configuration interaction (MRCI) model and an augmented correlation-consistent polarized valence quadruple zeta (aug-cc-pVQZ) basis set. For the neutral ground state of O_2 as well as for the real part of its anionic state O_2^-, the active space included the first 2 core orbitals ($1\sigma_g$, $2\sigma_g$) and 8 valence orbitals ($2\sigma_g$, $3\sigma_g$, $2\sigma_u$, $3\sigma_u$, $1\pi_u$, $1\pi_g$) plus 150 external orbitals for a total of 160 contractions. The MRCI orbitals were taken from a ground-state multiconfiguration self-consistent field (MCSCF) calculation in which 4 electrons were kept frozen in the core orbitals and excitations among all the valence orbitals were considered for the 12 and 13 electrons of the neutral and ionic states, respectively.

In the present work we update Noble *et al.*'s *R*-matrix calculations in order to have a better representation of the states involved in the scattering processes. Calculations were performed using the UKRMol codes [6]. Orbitals for O_2 were generated using configuration interaction (CI) calculations

*vincenzo.laporta@imip.cnr.it

using a correlation-consistent polarized valence triple zeta (cc-pVTZ) Gaussian-type orbital (GTO) basis set. The electrons in the lowest three core orbitals, $(1\sigma_g,2\sigma_g,1\sigma_u)^6$, were frozen, and an active space was constructed from nine valence orbitals $(3\sigma_g,2\sigma_u,3\sigma_u,1\pi_u,2\pi_u,1\pi_g)^{10}$. The scattering calculations with 17 electrons also used a GTO basis [7] to represent the continuum electron. The calculations were based on the use of a complete active space CI representation which involves placing the extra electron in both a continuum orbital and target orbitals using the following prescription: $(1\sigma_g, 2\sigma_g, 1\sigma_u)^6(3\sigma_g, 2\sigma_u, 3\sigma_u, 1\pi_u, 2\pi_u, 1\pi_g)^{11}$ and $(1\sigma_g, 2\sigma_g, 1\sigma_u)^6(3\sigma_g, 2\sigma_u, 3\sigma_u, 1\pi_u, 2\pi_u, 1\pi_g)^{10}(4\sigma_g, 5\sigma_g, 3\pi_u, 4\sigma_u, 2\pi_g, 3\pi_g, 1\delta_g, 1\delta_u)^1$, where the second set of configurations involves placing the extra electron in an uncontracted [8] target virtual orbital. Calculations used an R-matrix radius of $10a_0$. Both the MOLPRO and R-matrix calculations were performed using D_{2h} symmetry.

The potential curves calculated with the R-matrix and MOLPRO codes use different basis sets, different theoretical models, and different computational methods. This means that the resulting curves did not join, and a merging procedure was required. First of all, the O_2 neutral ground-state potential was calculated using MOLPRO, and all the subsequent results were referred to this curve. The real part of the resonance potentials, computed as a bound scattering state in the R-matrix calculations, was fixed at large internuclear distances beyond the crossing point to the MOLPRO curve which precisely reproduces the experimental oxygen atom electron affinity of 1.46 eV. At shorter internuclear distances, the R-matrix resonant curves are simply a smooth continuation of these large R curves, and therefore their positions are fixed by the corresponding MOLPRO curve. Potential-energy curves for the $O_2(X\,^3\Sigma_g^-)$ ground state, which supports 42 vibrational states, and the four resonance states plus the corresponding widths are reported in Fig. 1. We note that the new calculated potentials are slightly changed with respect to those of our previous paper [4], particularly for the $^2\Pi_u$ symmetry, and this could affect the RVE cross-section values. To check this aspect, we performed new calculations for RVE processes, observing, however, no significant changes in the cross sections with respect to the corresponding results in [4].

Previously [4], we showed that for energies up to about 4 eV the RVE cross sections are characterized by narrow spikes dominated by the $^2\Pi_g$ resonance. For energies of about 10 eV, the cross sections showed a broad maximum due to enhancement by the $^4\Sigma_u^-$ resonance with a smaller contribution coming from the $^2\Sigma_u^-$ state. In the case of DEA and EID processes we show that they are dominated, at least for low vibrational levels v of O_2, by the $^2\Pi_u$ resonance. Although electron attachment from oxygen molecules has been widely studied [9], there are only a few, rather old, papers reporting cross-section measurements of the DEA process as a function of the incident electron energy. We cite here Rapp and Briglia [10], Schulz [11], and Christophorou *et al.* [12]. DEA from the $^1\Delta_g$ state of O_2 has also been observed [13] and has been found to have a cross section of similar magnitude to process (1). Cross sections for EID appear to have been measured only for electronically excited states of O_2 by Cosby [14].

In the Born-Oppenheimer approximation, the dynamics of the oxygen nuclei in DEA is treated within the local-complex-potential model [15], which has already been satisfactorily adopted for resonant calculations in other diatomic molecules (see Refs. [4,16] and references therein). The corresponding cross section from the vibrational level v of oxygen and for electron energy ϵ is given by

$$\sigma_v(\epsilon) = 2\pi^2 \frac{m_e}{k}\frac{K}{\mu} \lim_{R\to\infty} |\xi(R)|^2, \qquad (3)$$

where K is the asymptotic momentum of the dissociating fragments O and O^- with reduced mass μ, m_e and $k = \sqrt{2m_e\epsilon}$ are the incoming electron mass and momentum, respectively, and $\xi(R)$ is the solution of the Schrodinger-like equation for the resonant state and total energy $E = \epsilon_v + \epsilon$:

$$\left(-\frac{\hbar^2}{2\mu}\frac{d^2}{dR^2} + V^- + \frac{i}{2}\Gamma - E\right)\xi(R) = -V\,\chi_v(R)\,, \qquad (4)$$

where $V^- + \frac{i}{2}\Gamma$ is the complex potential of the resonance reported in Fig. 1, $V^2 = \Gamma/(2\pi\,k)$ is the discrete-to-continuum potential coupling, and χ_v is the vibrational wave function of O_2 corresponding to the vibrational level v. R represents the internuclear distance. There is no interference among the resonant states with different symmetries, and for the two Σ_u^- states the interference can be considered to be negligible as they have different spin multiplicities.

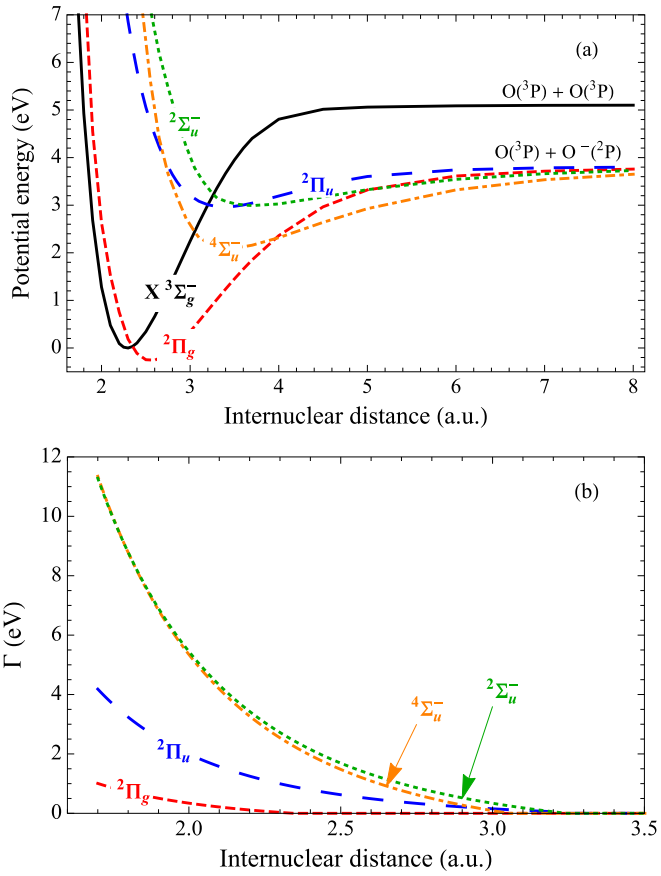

FIG. 1. (Color online) (a) Potential-energy curves for ground state $X\,^3\Sigma_g^-$ of O_2 and for the four lowest resonant states O_2^-. (b) The corresponding resonance widths $\Gamma(R)$ as a function of the internuclear distance.

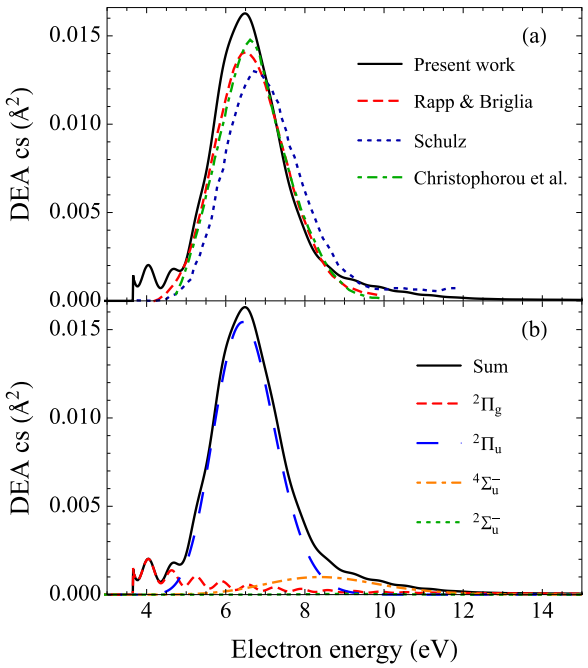

FIG. 2. (Color online) (a) Calculated dissociative electron attachment cross section for $v = 0$ compared with experimental results of Rapp and Briglia [10], Schulz [11], and Christophorou *et al.* [12]. (b) Contributions from the four resonances to the total cross section.

III. RESULTS AND DISCUSSION

Figure 2(a) shows our results for the DEA cross section for $O_2(v = 0)$ compared with the experimental results of Rapp and Briglia [10], Schulz [11], and Christophorou *et al.* [12]. The agreement is excellent, within the experimental error of $\pm 15\%$: the peak is positioned at 6.43 eV with an absolute value of 0.0154 Å^2 and FWHM of about 2 eV. Figure 2(b) reports cross sections from all four resonances and their sum. As found experimentally, the main contribution to DEA cross section comes from the $^2\Pi_u$ state of O_2^-. We also note, at about 8.5 eV, the presence of a significant contribution due to the $^4\Sigma_u^-$ symmetry which, added to the main $^2\Pi_u$ contribution, reproduces the high-energy tail observed experimentally. The non-negligible contribution of $^4\Sigma_u^-$ resonance to the DEA cross section has already been deduced from the measured angular distribution of O^- ions [17].

Figure 3 shows our DEA cross sections calculated for higher vibrational levels of O_2, $v = 10$,20 and 30, compared with the result $v = 0$. All cross sections are summed over all four resonance states. As expected [18], the threshold of the process shifts to lower energies as the vibrational level increases; this is due to the reduced threshold for dissociation limit. At the same time the maximum value of the cross section for $v < 30$ grows by of several orders of magnitude at low energies. This behavior is due to the survival factor $e^{-\rho}$ [19], given approximately by

$$e^{-\rho} \simeq \exp\left[-\int_{R_e}^{R_c} \frac{\Gamma(R)dR}{\hbar v(R)}\right], \qquad (5)$$

where integration is extended over the region between the classical turning point R_e and the stabilization point R_c and $v(R)$ is the classical velocity of dissociation. As the vibrational level increases, R_e increases, and the survival probability grows like the cross section. The oscillations, visible at high vibrational levels, result from the interplay between the neutral vibrational wave function and the resonant continuum wave function. Analysis of the resonance contributions to the cross section at $v = 20$ shows a complicated picture with both Π resonances making significant contributions at low energy and important contributions from the Σ resonances at higher energies.

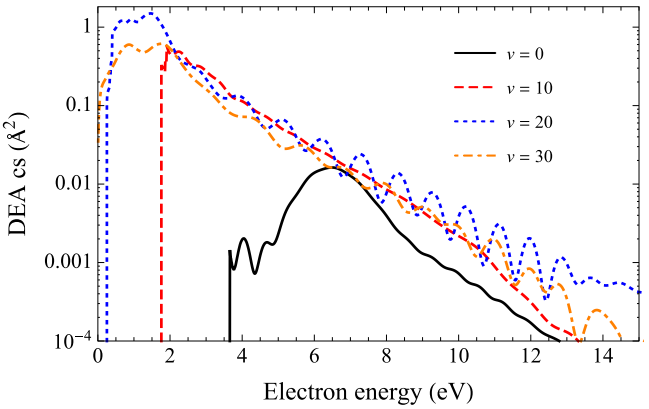

FIG. 3. (Color online) Calculated dissociative electron attachment cross sections for vibrationally excited O_2 for levels $v = 10$, 20, and 30 compared with the ground level $v = 0$. The cross sections include all four resonant contributions.

Figure 3 also shows the cross sections for $v = 30$. The increasing trend of the maxima is now inverted. The eigenvalue for this vibrational level [4], in fact, lies above the energy of the $O^-(^2P) + O(^3P)$ asymptotic state (see Fig. 1), so that the DEA process becomes exothermic with a threshold at zero energy. For this case $R_c > R_e$, so that the exponent ρ in Eq. (5) vanishes [$\Gamma(R > R_c) = 0$] and the magnitude of the cross section is no longer governed by the survival factor. The decreasing trend of the cross section maxima is maintained for $v > 30$.

The corresponding EID cross section from $O_2(X\,^3\Sigma_g^-; v)$ and electron energy ϵ is given by [16]

$$\sigma_v^{\mathrm{EID}}(\epsilon) = \frac{64\pi^5 m^2}{\hbar^4} \int d\epsilon' \frac{k'}{k} |\langle \chi_{\epsilon'}(R)|V|\xi(R)\rangle|^2 , \qquad (6)$$

where $\langle \cdots \rangle$ means integration over the internuclear distance R, $\xi(R)$ is the resonant wave function solution of Eq. (4), and $\chi_{\epsilon'}$ is the continuum wave function of O_2 with energy ϵ' representing the $2O + e^-$ fragments. The continuum energy ϵ' was integrated from the O_2 dissociation threshold up to 10 eV.

Figure 4(a) shows the calculated EID cross sections for $v = 0$. Contributions coming from the four O_2^- resonances are shown. Like DEA, the main contribution comes from the $^2\Pi_u$ symmetry, which gives a maximum at 6.93 eV with an absolute value of 0.0072 Å^2, and there is a significant contribution from the $^4\Sigma_u^-$ at 9.47 eV with a cross section of 0.0026 Å^2. The contribution from the other symmetries is negligible. Figure 4(b) shows the cross sections for excited vibrational levels of oxygen compared with those for the ground level. Cross sections include all four resonance contributions. As expected [18], the EID cross section increases rapidly with vibrational excitation, and the threshold moves to lower energy.

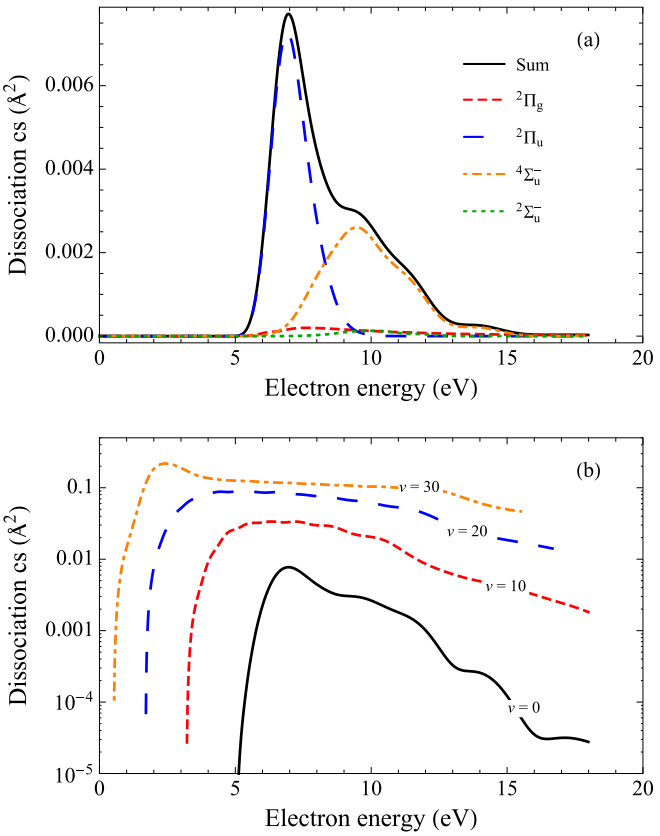

FIG. 4. (Color online) (a) Calculated cross sections for resonant electron impact dissociation of oxygen for $v = 0$. Contributions from the four O_2^- resonances are shown; the black curve is the sum. (b) Dissociating cross sections for vibrationally excited oxygen at $v = 10$, 20, and 30 compared with the results for $v = 0$.

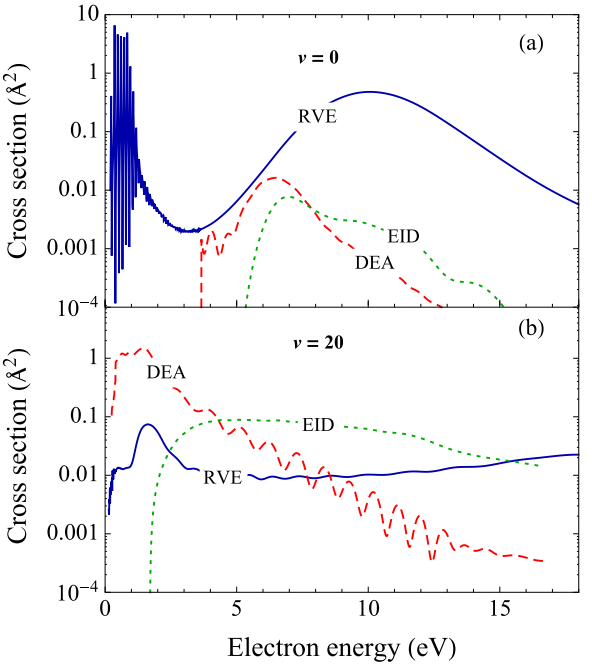

FIG. 5. (Color online) Summary of the cross sections for electron-O_2 collisions: Resonant vibrational excitation for $\Delta v = 1$ transition [4] (solid line), dissociative electron attachment (long-dashed line), and resonant dissociation by electron impact (short-dashed line) for (a) $v = 0$ and (b) $v = 20$. The cross sections are the sum over the four O_2^- resonances.

The cross section for $v = 30$, for example, reaches a value comparable to that of the well-known Schumann-Runge dissociative transitions for the same vibrational level [20], whose dissociative cross sections decrease with increasing vibrational excitation of the molecule. We note that EID is known to occur efficiently via electron impact excitation of O_2 [1,9]. However, the threshold for electronic excitation processes lies significantly higher than those considered here, making them relatively unimportant in low-temperature plasmas.

IV. CONCLUSIONS

In conclusion, we present calculations for dissociative electron attachment for oxygen using *ab initio* potential-energy curves and calculations for resonant electron-impact dissociation of oxygen. We confirm the dominant contribution of $^2\Pi_u$ symmetry in both processes starting from $v = 0$. Both cross sections, however, increase rapidly with an increase in the vibrational excitation of the molecule, and for these vibrationally excited states it is necessary to consider the contributions from all four of the low-lying O_2^- resonance states.

Finally, Fig. 5 compares cross sections for different resonant processes involving electron-$O_2(X\,^3\Sigma_g^-, v)$ scattering: our previous results for $v \rightarrow v + 1$ vibrational excitation [4] and the present cross sections for DEA and EID for the cases when O_2 is initially in its vibrational ground state and in its $v = 20$ state. For the $v = 0$ level vibrational excitation is the dominant low-energy process. However, for vibrationally excited molecules the DEA increases rapidly and becomes the most important process at low energies. We expect that the inclusion of these results will have important consequences in models of plasmas containing molecular oxygen and, in particular, will lead to a significant increase in O^- ion production in these models.

Recently, we also calculated the rate coefficients for processes (1) and (2) as a function of the electronic temperature and for all the vibrational levels. Details of the calculations and results are reported in [21]. DEA and EID cross sections as a function of electron energy and O_2 vibrational state, along with the corresponding rate coefficients, have been made freely available in the Phys4Entry database [22].

ACKNOWLEDGMENTS

The authors are grateful to Prof. M. Capitelli (Università di Bari and IMIP-CNR Bari, Italy) for useful discussion and comments on the manuscript. This work was performed as part of the Phys4Entry project under EU FP7 Grant Agreement No. 242311. One of the authors (R.C.) would like to acknowledge financial support from Ministero dell'Istruzione, dell'Università e della Ricerca (MIUR)-PRIN 2010-11, Grant No. 2010ERFKXL.

[1] Y. Itikawa, J. Phys. Chem. Ref. Data **38**, 1 (2009).
[2] C. J. Noble, K. Higgins, G. Wöste, P. Duddy, P. G. Burke, P. J. O. Teubner, A. G. Middleton, and M. J. Brunger, Phys. Rev. Lett. **76**, 3534 (1996).
[3] J. Tennyson, Phys. Rep. **491**, 29 (2010).
[4] V. Laporta, R. Celiberto, and J. Tennyson, Plasma Sources Sci. Technol. **22**, 025001 (2013).
[5] H.-J. Werner, P. J. Knowles, G. Knizia, F. R. Manby, and M. Schütz, WIREs Comput. Mol. Sci. **2**, 242 (2012).
[6] J. M. Carr, P. G. Galiatsatos, J. D. Gorfinkiel, A. G. Harvey, M. A. Lysaght, D. Madden, Z. Masin, M. Plummer, and J. Tennyson, Eur. Phys. J. D **66**, 58 (2012).
[7] A. Faure, J. D. Gorfinkiel, L. A. Morgan, and J. Tennyson, Comput. Phys. Commun. **144**, 224 (2002).
[8] J. Tennyson, J. Phys. B **29**, 6185 (1996).
[9] J. McConkey, C. Malone, P. Johnson, C. Winstead, V. McKoy, and I. Kanik, Phys. Rep. **466**, 1 (2008).
[10] D. Rapp and D. D. Briglia, J. Chem. Phys. **43**, 1480 (1965).
[11] G. J. Schulz, Phys. Rev. **128**, 178 (1962).
[12] L. G. Christophorou, R. N. Compton, G. S. Hurst, and P. W. Reinhardt, J. Chem. Phys. **43**, 4273 (1965).
[13] T. Jaffke, M. Meinke, R. Hashemi, L. G. Christophorou, and E. Illenberger, Chem. Phys. Lett. **193**, 62 (1992).
[14] P. C. Cosby, J. Chem. Phys. **98**, 9560 (1993).
[15] W. Domcke, Phys. Rep. **208**, 97 (1991).
[16] V. Laporta, D. Little, R. Celiberto, and J. Tennyson, Plasma Sources Sci. Technol. **23**, 065002 (2014).
[17] V. S. Prabhudesai, D. Nandi, and E. Krishnakumar, J. Phys. B **39**, L277 (2006).
[18] D. T. Stibbe and J. Tennyson, New J. Phys. **1**, 2 (1998).
[19] T. F. O'Malley, Phys. Rev. **155**, 59 (1967).
[20] A. Laricchiuta, R. Celiberto, and M. Capitelli, Chem. Phys. Lett. **329**, 526 (2000).
[21] V. Laporta, R. Celiberto, and J. Tennyson, AIP Conf. Proc. **1628**, 939 (2014).
[22] Database of the European Union Phys4Entry project, 2012–2014, http://users.ba.cnr.it/imip/cscpal38/phys4entry/database.html.